Inorganic Chemistry

pubs.acs.org/IC

Article

Scalable Synthesis of Selenide Solid-State Electrolytes for Sodium-Ion Batteries

Saeed Ahmadi Vaselabadi, Katie Palmer, William H. Smith, and Colin A. Wolden*

Cite This: *Inorg. Chem.* 2023, 62, 17102−17114

Read Online

ACCESS | Metrics & More | Article Recommendations | Supporting Information

ABSTRACT: Solid-state sodium-ion batteries employing superionic solid-state electrolytes (SSEs) offer low manufacturing costs and improved safety and are considered to be a promising alternative to current Li-ion batteries. Solid-state electrolytes must have high chemical/electrochemical stability and superior ionic conductivity. In this work, we employed precursor and solvent engineering to design scalable and cost-efficient solution routes to produce air-stable sodium selenoantimonate (Na_3SbSe_4). First, a simple metathesis route is demonstrated for the production of the Sb_2Se_3 precursor that is subsequently used to form ternary Na_3SbSe_4 through two different routes: alcohol-mediated redox and alkahest amine-thiol approaches. In the former, the electrolyte was successfully synthesized in EtOH by using a similar redox solution coupled with Sb_2Se_3, Se, and NaOH as a basic reagent. In the alkahest approach, an amine-thiol solvent mixture is utilized for the dissolution of elemental Se and Na and further reaction with the binary precursor to obtain Na_3SbSe_4. Both routes produced electrolytes with room temperature ionic conductivity (~0.2 mS cm^{-1}) on par with reported performance from other conventional thermo-mechanical routes. These novel solution-phase approaches showcase the diversity and application of wet chemistry in producing selenide-based electrolytes for all-solid-state sodium batteries.

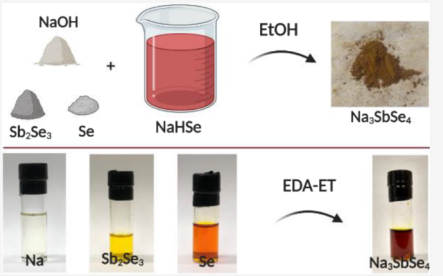

INTRODUCTION

Chalcogenides are a diverse and essential class of compounds that are employed in a variety of energy applications including photovoltaic[1,2] and thermoelectric energy conversion,[3] as well as energy storage media such as batteries and fuel cells.[4,5] Specifically, ternary and quaternary chalcogenides are widely explored as solid-state electrolyte and cathode materials for lithium and sodium-ion batteries.[4−8] Sodium-ion batteries are garnering enormous attention for large-scale energy storage and power grid applications owing to their low cost, enhanced sustainability, and good performance. Replacing conventional liquid electrolytes with solid-state electrolytes enhances the thermal stability and innate safety of all-solid-state Na-ion batteries. In addition, the incorporation of Na as the anode is expected to improve energy density and prevent dendrite formation.[9−11]

However, to date, the performance of solid-state electrolytes faces various challenges such as low ionic conductivity (σ_{Na+}), poor air stability, and interfacial incompatibility with the electrodes.[12,13] Among the various classes of SSEs, inorganic Na-based solid-state electrolytes and specifically ternary chalcogenides and their derivatives are promising candidates that can achieve high ionic conductivity and mechanical ductility compared with oxide-based electrolytes such as Na beta-alumina and NASICONs. Oxides suffer from interfacial resistance and grain boundary contribution at room temperature (RT) cold pressing and typically require very high-temperature sintering to provide a similar ionic conductivity. Alternatively, chalcogenides can be incorporated into a cell through simple cold pressing at ambient temperature.[13−15]

The tetragonal phase of Na_3PS_4 (σ_{Na+} = 0.004 mS cm^{-1}), the archetype of Na-based sulfide electrolytes, was first synthesized by Jansen and Henseler.[16] Later Hayashi and co-workers[17] prepared the highly conductive (0.2 mS cm^{-1}) cubic phase through high-energy mechanical milling. Since then, research efforts have produced a variety of iso/aliovalent-doped sulfides such as Na_3MS_4,[18−22] $Na_{11}Sn_2MS_{12}$[23,24] (M = P, Sb), $Na_{2.9375}PS_{3.9375}Cl_{0.0625}$,[25] $Na_3P_{0.62}As_{0.38}S_4$,[26] $Na_{2.730}Ca_{0.135}PS_4$[27] and so on via various synthesis methods. Remarkably, Hayashi et al.[28] and Fuchs et al.[29] showed that tungsten-doped Na_3SbS_4 can achieve very high ionic conductivity surpassing the performance of liquid electrolytes (>10 mS cm^{-1}). This performance was mainly attributed to the formation of defects resulting from the addition of Na vacancy to the host lattice. In terms of air stability, phosphorus-containing electrolytes do react with oxygen and water moisture, leading to the release of toxic H_2S gas and subsequent loss of structure and performance. Therefore, the addition/replacement of phosphorus with softer acids such as Sn^{4+} and Sb^{5+} has been demonstrated to

Received: June 1, 2023
Published: October 12, 2023

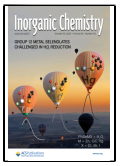

https://doi.org/10.1021/acs.inorgchem.3c01799
Inorg. Chem. 2023, 62, 17102−17114

provide a more stable bonding between the central cation and sulfide ion based on Pearson Hard and soft acid and base (HSAB) theory.[30]

Replacement of sulfide with selenide anions can expand the crystal lattice due to selenide's larger ionic radius while decreasing the binding energy between the anionic lattice framework and Na ions because of its high polarizability. This is specifically more beneficial in Na-based compounds compared to Li counterparts since selenides provide larger diffusion channels suiting the larger Na^+ ions diffusion requirements leading to improved ionic transport.[31−33] Furthermore, studies from the Zeier group[34,35] showed that softening the lattice by incorporating more polarizable Se in the Na_3MS_4 (M = P, Sb) system will lower the activation barrier and Arrhenius prefactor. Similar attempts were made to synthesize more air-stable Se-doped Na_3SbS_4 electrolytes that led to the production of cubic Na_3SbSe_4 with a high conductivity of 0.85 mS cm^{-1} and improved activation barrier (0.19 eV) relative to its sulfide analog.[36] A later study by Wang and co-workers[37] investigated the Sb doping in the parent Na_3PSe_4 system and reported a remarkable 3.7 mS cm^{-1} conductivity with similar activation energy as previous reports.

Like other ceramic electrolytes, conventional synthesis routes of selenides include mechanochemistry and high-temperature solid-state reactions, which are often time- and energy-intensive. Solution-based synthesis of selenide SSEs has not been explored in detail yet. Organic solvents utilized in this approach partially or fully dissolve the precursors driving the reaction through "suspension/solution" allowing us to control particle size and morphology of the resulting SSE product.[38,39] To date, most of the reported liquid-based techniques have been focused on sulfides. Selenides are far more challenging due to a lack of appropriate solvents that could either dissolve selenium or facilitate the selenide formation reaction in the suspension form. In our previous report,[22] we demonstrated ethanol as a benign and environment-friendly solvent that can be used to produce Na_3SbS_4 with improved yield and high ionic conductivity. This has inspired us to study various solvent systems, including ethanol and other mixtures, that could produce ternary selenides without any undesired side reactions.

In this work, we report two wet-chemical synthesis approaches for the highly air-stable sodium selenoantimonate, Na_3SbSe_4. First, we demonstrate the redox reaction of binary Sb_2Se_3 that was employed as a precursor for the production of ternary Na_3SbSe_4 in polar solvents such as water and ethanol via suspension synthesis. Second, we use the mixture of relatively volatile and benign solvents, that is, ethylene diamine (EDA)- ethanethiol (ET), to synthesize Na_3SbSe_4 based on a solution approach, which can be recovered with no carbonization at mild temperatures. The underlying chemistry and impurity profile of each approach was elucidated through a complementary set of physical characterization techniques including scanning electron microscopy (SEM), X-ray diffraction (XRD), Raman, and Fourier transform infrared (FTIR) spectroscopy. The electrochemical performance of the obtained SSE including ionic conductivity, activation energy, and electrochemical stability against Na-alloy anode was determined through electrochemical impedance spectroscopy (EIS) and galvanostatic cycling. This work introduces various solution-phase syntheses of ternary selenides that will expand the strategies available to produce this important class of chalcogenides.

EXPERIMENTAL SECTION

Materials. Antimony chloride ($SbCl_3$, ACS, 99% min, Alfa Aesar), sodium borohydride ($NaBH_4$, > 98%, Sigma-Aldrich), selenium (Se, 99.99%, UMC), sodium (Na, Sigma-Aldrich), tin powder (Sn, Alfa Aesar, −325mesh, 99.8%), ethanol (EtOH, Sigma-Aldrich, anhydrous, ⩾99.5%), 1, 2-ethylenediamine (EDA, Alfa Aesar, 99%), ethanethiol (ET, Sigma-Aldrich, 97%), and UHP grade argon (Ar, 99.999%, General Air) were used as received without purification. Se pellets were further ground using a mortar and pestle to reduce particle size. All procedures were conducted in an Ar-filled glovebox (<1 ppm of H_2O) except otherwise stated.

Synthesis. *Sb_2Se_3.* Sb_2Se_3 was synthesized in ∼2 g batches as follows. First, the $NaBH_4$ solution was prepared by adding 1212 mg (32.0 mmol) of $NaBH_4$ in 40 mL of DI water and stirring for 1 h to fully dissolve. Next, $NaBH_4$ solution was added dropwise to 1150 mg (14.6 mmol) of Se in a three-neck flask that could facilitate the release of the redox reaction byproduct hydrogen gas. After stirring for 2 h at RT, a clear solution of NaHSe was formed. 10% excess $NaBH_4$ was used to ensure the full reduction of Se powder. In another container, 2215 mg (9.7 mmol) of $SbCl_3$ was dissolved in 20 mL EtOH. Then, the $SbCl_3$ solution was slowly added to the aqueous NaHSe and stirred overnight to ensure reaction completion. The as-obtained product was centrifuged and washed with water and EtOH consecutively multiple times and dried at RT for 12 h in a vacuum. An extra step of precipitate grinding and dispersion in water was performed to remove the NaCl byproduct. The final yield was ∼83%. The recovered powder was annealed under Ar flow at 200, 300, and 400 °C in a horizontal tube furnace with a heating rate of 5 °C min^{-1} to remove the residual solvents and form the crystalline Sb_2Se_3.

Aqueous Na_3SbSe_4 (R1). 250 mg (6.6 mmol) of $NaBH_4$ in 2 mL of water was slowly added to 250 mg (3.1 mmol) of Se at RT to prepare the aqueous NaHSe. After 1 h of reaction, the solution was cooled down to 4 °C and centrifuged to collect and discard the precipitate. Next, 500 mg (1.0 mmol) of Sb_2Se_3, 130 mg (3.2 mmol) of NaOH, and 164 mg (2.2 mmol) of Se were added to the aqueous NaHSe solution. The dark suspension turned to light brown very quickly and was stirred overnight. After centrifugation, the solid product was collected by drying the supernatant at 150 °C in a tubular furnace under continuous Ar flow for 2 h. The yield was roughly 67%.

0.5 M Ethanolic NaHSe Stock Solution. 1040 mg (27.5 mmol) of $NaBH_4$ was dissolved in 50 mL of EtOH and slowly added to 1972.4 mg (25.0 mmol) of Se powder in a 100 mL flask. 10% excess $NaBH_4$ was used to ensure the full reduction of Se powder. The solution was later filtered to remove any unreacted Se.

Aqueous Ethanolic Na_3SbSe_4 (R2). 47.2 mg (1.25 mmol) of $NaBH_4$ was dissolved in 2.5 mL of EtOH and slowly added to 98.6 mg (1.25 mmol) of Se powder in a flask to form the ethanolic NaHSe solution. 7.5 mL of H_2O, 200 mg (0.42 mmol) of Sb_2Se_3, 50 mg (1.25 mmol) of NaOH, and 65.7 mg (0.83 mmol) of Se were added to this flask. The water/EtOH ratio was set at 3. After stirring overnight, the undissolved precipitate was discarded, while the supernatant was dried at 150 °C for 2 h under Ar flow in a tube furnace.

Ethanolic Na_3SbSe_4 (R3). To prepare "R3, 1× NaHSe" electrolyte, 400 mg (0.82 mmol) of Sb_2Se_3, 100 mg (2.50 mmol) of NaOH, and 131.5 mg (1.67 mmol) of Se were added to 5 mL of 0.5 M ethanolic. The solution was stirred overnight, decanted, and washed with EtOH twice. The precipitate was dried overnight under vacuum at RT. For the "R3, 2× NaHSe" experiment, 10 mL of 0.5 M ethanolic NaHSe and 200 mg (5 mmol) of NaOH to ensure neutrality was used. The electrolyte yield was ∼83%. Ethanolic Na_3SbSe_4 was further heat-treated at various temperatures for 2 h under flowing Ar in a custom-built fluidized-bed drier.

EDA Synthesis of Na_3SbSe_4. 400 mg (0.82 mmol) of Sb_2Se_3, 115 mg (5 mmol) of Na, and 329 mg (4.16 mmol) of Se were added to 10 mL of EDA and reacted at 90 °C on a hot plate inside the glovebox for 1 day. Reflux reaction was performed in a round-bottom flask attached to a condenser at 130 °C for 1 day under continuous Ar flow (10 sccm flow). After the reaction, the solutions were centrifuged, and

https://doi.org/10.1021/acs.inorgchem.3c01799
Inorg. Chem. 2023, 62, 17102−17114

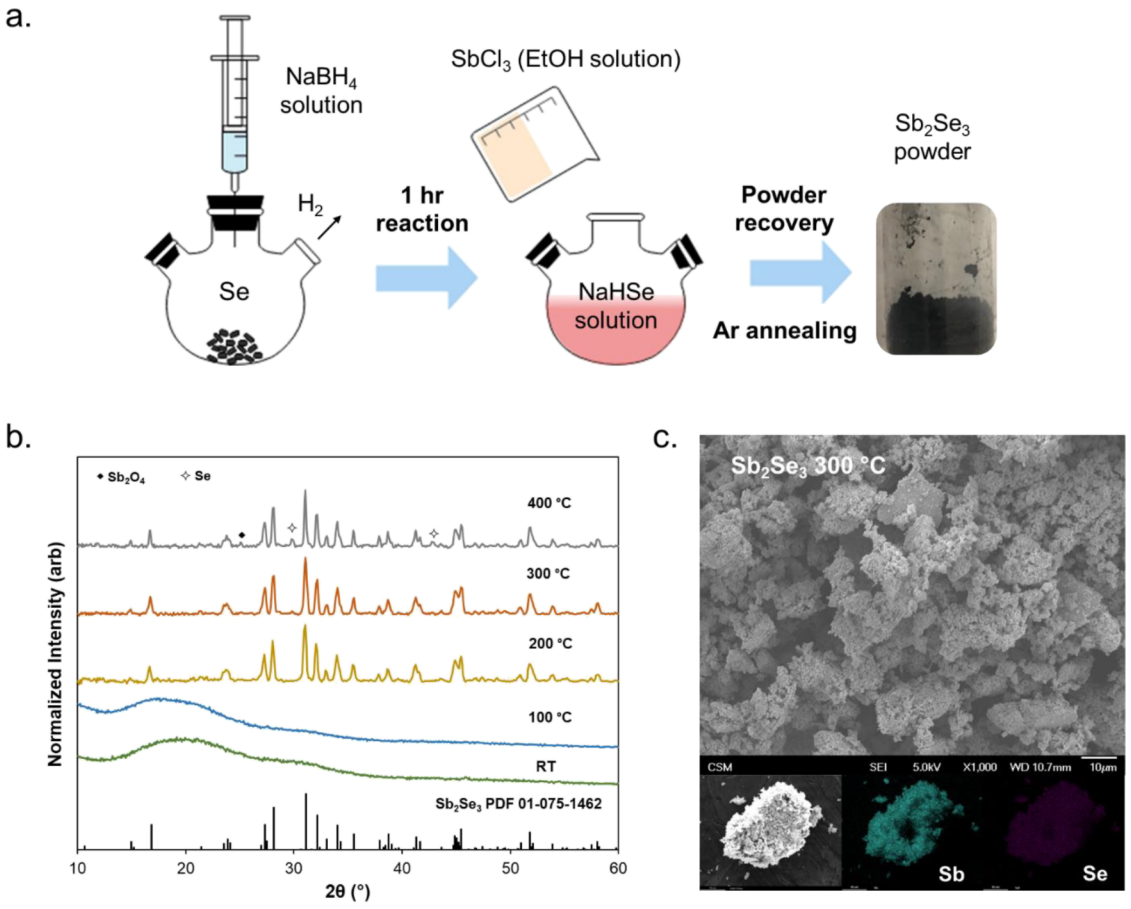

Figure 1. (a) Schematic of Sb_2Se_3 metathesis process, (b) diffraction patterns of metathesis products heat-treated at different temperatures. The reflections at the 200 °C annealing sample are assigned to the orthorhombic phase of Sb_2Se_3. (c) SEM image and EDX elemental mapping of crystalline Sb_2Se_3 powder.

the collected supernatant was dried at 150 °C for 2 h under Ar flow in a tube furnace.

EDA-ET Synthesis of Na_3SbSe_4. 400 mg (0.82 mmol) of Sb_2Se_3, 115 mg (5 mmol) of Na, and 329 mg (4.16 mmol) of Se were dissolved and reacted in 10 mL of EDA-ET (4:1 v/v) at RT inside the glovebox. After 1 day, the EDA-ET solution was centrifuged, and the collected supernatant was dried at 150 °C for 2 h under Ar flow in a tube furnace. Recovered Na_3SbSe_4 was further heat-treated at various temperatures for 2 h under flowing Ar in a custom-built fluidized-bed drier. The product yield was ∼85%.

Precursor Solubility. We also attempted to quantify the solubility of individual precursors in a 4:1 v/v mixture of EDA: ET. The solubility limits were measured by adding aliquots of precursor powders in 1 mL of EDA-ET with continuous stirring for a few hours until no dissolution and saturation are discerned visibly. Sb_2Se_3, Se, and Na were soluble up to ∼1.5 (7.5), ∼4.4 (3.5), and ∼1.8 (0.42) mol L^{-1} (wt %), respectively, when dissolved at room temperature (Figure 4c). Weber and Brutchey[40] reported a 28 wt % solubility of Sb_2Se_3 in a 10:1 1,2-ethylenediamine and 1,2 ethanedithiol solution, which is higher than our measured value most likely due to the strong deprotonating ability of dithiol compared monothiol solvents.

Material Characterization. Thermogravimetric analysis (TGA) was performed on a TA Instruments SDT-Q650 model. For a typical run, 10 mg of sample was loaded into a precleaned alumina pan and heated under flowing Ar from RT to 400 °C at 10 °C min^{-1} rate and then cooled down naturally. X-ray diffraction (XRD) was performed with a Philips X'Pert X-ray diffractometer with Cu Kα radiation (λ = 0.15405 nm) between 10° and 60° at a scan rate of 3° min^{-1}. Samples were prepared on a glass slide with protective tape covering the material to prevent undesired reactions with ambient air. XRD background correction and Rietveld refinement were performed using HighScore software. Raman spectroscopy was conducted with a WiTec alpha 300 M Confocal Microscope/Raman Spectrometer employing a 100 mW 532 nm laser. Samples were mounted on a glass slide and sealed under a 0.1 mm quartz coverslip. The laser was focused through the coverslip onto the sample using a 20× objective, and spectra were collected using a CCD detector (Andor Technologies) at −60 °C. Fourier-transform infrared spectroscopy (FTIR) was performed with a Nicolet Summit FT-IR spectrometer using an attenuated total reflection (ATR) accessory equipped with a diamond crystal. Field emission scanning electron microscopy (FESEM) images were collected on a JEOL JSM-7000F FESEM instrument equipped with energy-dispersive X-ray spectroscopy (EDX) for compositional analysis. To prepare the samples for SEM and EDX measurements, powder samples were immobilized onto an aluminum stub by using double-sided carbon tape. An accelerating voltage of 5 kV was used for taking the SEM image while a higher voltage of 15−20 V was employed for EDX spectra collection. All sample preparation was done in an Ar glovebox.

Electrochemical Characterization. Pellets of Na_3SbSe_4 electrolytes were prepared for conductivity measurements via conventional uniaxial pressing. For this purpose, 150−250 mg of the electrolyte was loaded into a 12 mm PEEK split cell with stainless steel plungers under a uniaxial fabrication pressure of 270 MPa and held for 5 min. Pellets were typically 0.6−0.8 mm thick (∼75 to 90% densification). The SSE pellets were contacted using stainless steel plungers as ion-blocking electrodes for electrochemical characterization. The pressure was released for 1 min and then increased again to 75 MPa. A Gamry Interface 1000E potentiostat was used to perform electrochemical impedance spectroscopy (EIS) measurements across a frequency

https://doi.org/10.1021/acs.inorgchem.3c01799
Inorg. Chem. 2023, 62, 17102−17114

range of 1 Hz to 1 MHz with a 10 mV perturbation. Temperature-dependent EIS testing was performed by heating the split cell apparatus with an electrical heating element and allowing it to stabilize at the target temperature for 1.5 h. The accuracy of the temperature control was verified by measuring the surface temperature of the sample with a thermocouple inserted in the split cell. DC polarization measurements were performed by applying three-step potentials to the sample (0.6, 0.8, and 1 V) and recording the transient current. The steady-state current was recorded after 2 h at each step potential, and the electrical conductivity was calculated using Ohm's law.

Sodium plating/stripping cycling was performed in a symmetrical $Na_{15}Sn_4|Na_3SbSe_4|Na_{15}Sn_4$ cell at a current density of 0.02 mA cm^{-2}. $Na_{15}Sn_4$ was synthesized by milling the stoichiometric amounts of finely cut Na and Sn powder (total mass of ~750 mg) in a planetary mill (Across International, PQN2) at 350 rpm for 10 h. To assemble the symmetric cell, 150 mg of Na_3SbSe_4 (R3, 2× NaHSe) was cold-pressed in a PEEK split cell at 270 MPa. Then, 60 mg of $Na_{15}Sn_4$ powders were dispersed on both sides of the Na_3SbSe_4 pellet and cold-pressed together at 340 MPa for 5 min. Galvanostatic charging and discharging (30 min per step) was performed after aging the cell at 60 °C for 2 h by a battery tester (MTI Corporation, BST8-MA) with a stacking pressure of 50 MPa. A Gamry Interface 1000E potentiostat was used to measure the EIS spectra at different cycling intervals.

RESULTS AND DISCUSSION

Sb_2Se_3 Preparation. Binary Sb_2Se_3 is a promising chalcogenide with unique optical and electrical properties that finds applications in photovoltaics,[41] photoelectrochemical water splitting,[42] and battery electrodes.[43−45] Sb_2Se_3 is one of the main cost-driver precursors in the synthesis of Sb-based selenides (38.6 $/g, Sigma-Aldrich),[46] therefore, we developed a simple cost-efficient synthesis of bulk Sb_2Se_3 without the use of solvothermal processing. The target product was produced through a metathesis-based redox reaction in an aqueous solution at room temperature, as illustrated in Figure 1a. In this process, the common reduction agent $NaBH_4$ was used to convert elemental Se into sodium hydrogen selenide, NaHSe, which was further reacted with $SbCl_3$ dissolved in EtOH via counterion exchange reaction to produce Sb_2Se_3 (eqs 1−2).[47,48] This reduction is spontaneous and favorable at RT. NaCl and other impurities including sodium tetraborate ($Na_2B_4O_7$) or borax are washed away during the purification step, and black precipitates were recovered after drying under vacuum at RT overnight.

$$2Se_{(s)} + 4NaBH_{4(sol)} + 7H_2O_{(l)} \rightarrow 2NaHSe_{(sol)} + Na_2B_4O_{7(sol)} + 14H_{2(g)} \quad (1)$$

$$3NaHSe_{(sol)} + 2SbCl_{3(sol)} \rightarrow Sb_2Se_{3(s)} + 3NaCl_{(sol)} + 3HCl_{(sol)} \quad (2)$$

This approach was inspired by the redox reaction used by Guo et al.[44] without the need for a capping agent and high energetics of the solvothermal approach (i.e., high pressure and temperature). Figure 1b displays the XRD patterns of precipitates collected from the metathesis reaction. The precipitate is fully amorphous with no traces of other crystalline side products indicating the complete removal of NaCl. The supernatant was also evaporated to further confirm the removal of NaCl salt (Figure S1). Heat treatment of the precipitate under an Ar atmosphere results in the crystallization of Sb_2Se_3 into a pure orthorhombic phase with *Pbnm (62)* space group (PDF 01-075-1462) at 200 °C.[48,49] This is in good agreement with literature reports stating 161 °C as the onset of crystallization and 188 °C to fully crystallize the amorphous thin films of Sb_2Se_3.[50] Increasing the heat treatment temperature enhances the crystallinity of the samples demonstrated by narrow and sharper peaks; however, it raises the probability of oxidation/decomposition as well. The sample heat-treated at 400 °C shows the presence of a trace amount of Sb_2O_4 and Se possibly due to the decomposition of binary selenide.[43] Hence, Sb_2Se_3 heat-treated at 300 °C with the highest crystallinity and minimum impurities is employed for further characterization and as the precursor to the subsequent electrolyte reaction.

SEM was used to investigate the morphology and microstructure of Sb_2Se_3. Figure 1c shows the SEM images and the corresponding EDX element mapping of the Sb_2Se_3 sample annealed at 300 °C, demonstrating a uniform distribution of elements within the crystalline material. A semiquantitative EDX analysis (Figure S2) shows the Se/Sb stoichiometric ratio of ~1.49. SEM micrograph shows agglomerated microstructures of 10−50 μm; lack of capping agents most likely leads to the low control over size and formation of inhomogeneous larger particles. Various morphologies with better control on size through applying capping agents have been shown to improve the electrochemical properties of Sb_2Se_3 utilized as an anode in Na/Li-ion batteries; however, the primary morphology of the Sb_2Se_3 precursors was not of particular interest in this synthesis. Here we showed that Sb_2Se_3 can be produced through a room-temperature reaction without the need to use solvothermal energetics. Also, this approach uses a more benign, environmental-friendly, and more cost-efficient precursor such as $NaBH_4$ and $SbCl_3$ compared to other methods incorporating toxic hydrazine and other antimony salts such as acetates.[45]

Alcohol-Mediated Synthesis of Na_3SbSe_4. Inspired by the applicability of NaHSe as a reagent in producing Sb_2Se_3, we explored the possibility of leveraging this Se ion source in developing ternary selenides in protic solvents, such as water and ethanol. This process consists of a redox reaction to form NaHSe followed by a final electrolyte reaction in which the rest of the precursors, Sb_2Se_3, excess Se, and NaOH as a basic agent, are added (Figure 2). Like Sb_2Se_3 synthesis, an aqueous

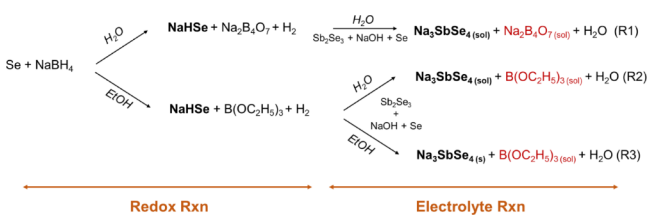

Figure 2. Reaction schemes for aqueous- and alcohol-mediated synthesis of Na_3SbSe_4 electrolytes.

NaHSe solution that contains borax as a side product is formed in water (eq 1). As the ternary electrolyte is soluble in water, the formed borax will precipitate out during the powder recovery with the electrolyte; therefore, a separation step is needed to minimize the borate concentration. For this purpose, the NaHSe solution was cooled to 4 °C and the borate precipitate was removed through centrifugation.[47,51] Based on the mild solubility of borax in water, complete removal is not viable, so there still will be traces of borax

https://doi.org/10.1021/acs.inorgchem.3c01799
Inorg. Chem. 2023, 62, 17102−17114

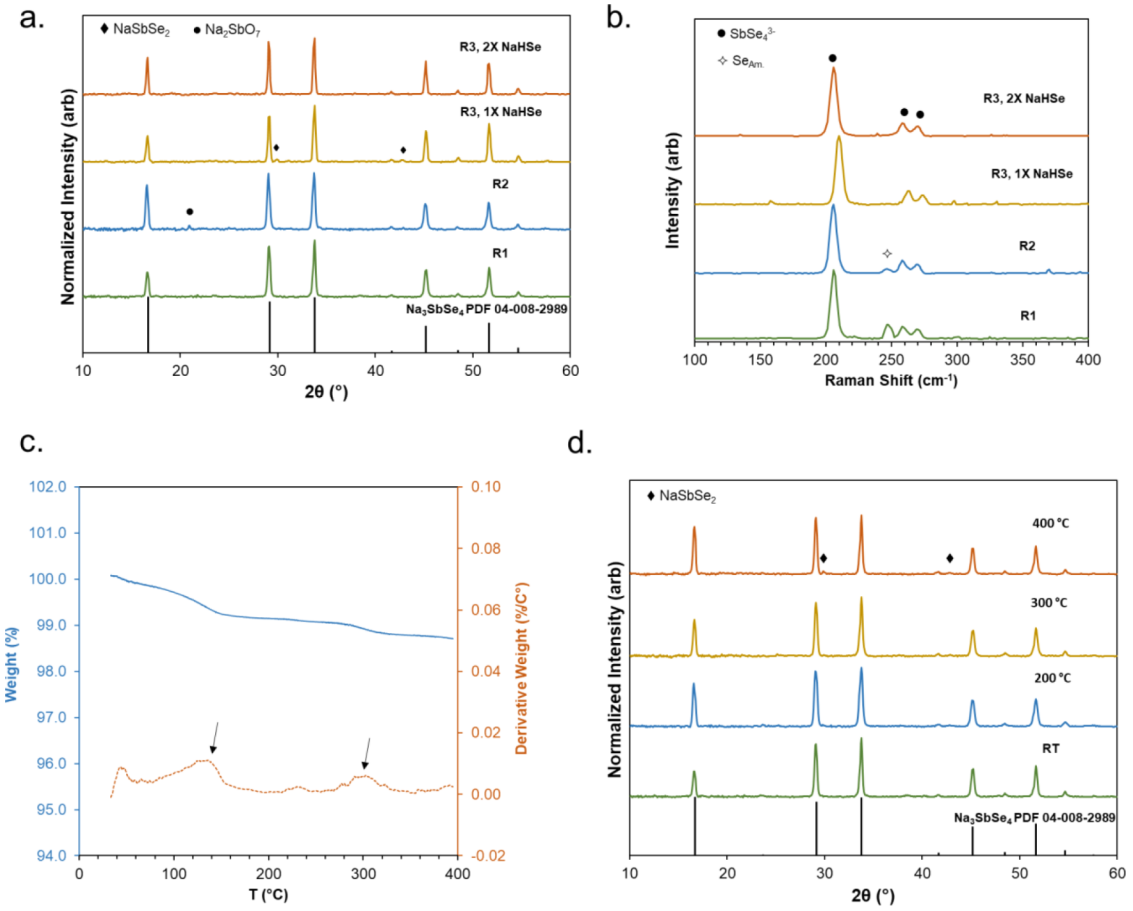

Figure 3. (a) XRD and (b) Raman spectra of Na_3SbSe_4 derived from H_2O, EtOH, and their mixed solutions. Aqueous and aqueous-ethanolic solutions were evaporated at 150 °C (Ar) while precipitates recovered from EtOH dried at RT under vacuum. (c) TGA scan of ethanolic Na_3SbSe_4 (R3, 2× NaHSe) and (d) diffraction pattern of ethanolic Na_3SbSe_4, (R3, 2× NaHSe), heat-treated at 200, 300, and 400 °C under Ar.

present in the solution. Next, Sb_2Se_3, Se, and NaOH are added to aqueous NaHSe to proceed with the formation of Na_3SbSe_4. This reaction path is denoted as R1. The dark suspension quickly turned into a brown solution. The electrolyte is recovered by centrifugation and drying at 150 °C in Ar atmosphere. The undissolved species are discarded.

We previously showed that ethanol can be used as a benign solvent to synthesize Na_3SbS_4, and considering a similar molecular chemistry of the sulfides and selenides, we postulated that the EtOH could drive the Na_3SbSe_4 reaction toward completion as well.[22] Additionally, it was stated that the reduction of Se with $NaBH_4$ in a less polar EtOH is more favorable as the rate of $NaBH_4$ decomposition is significantly slower compared to water-mediated reduction. This improves the yield of the final material with regard to the amount of borohydride consumed (eq 3). Most importantly, this solution can be utilized directly in different reactions such as Na_3SbSe_4 formation since triethyl borate ($B(OC_2H_5)_3$) is fairly inactive and will not impact the main reaction.[47,52]

$$Se_{(s)} + NaBH_{4(sol)} + 3C_2H_5OH_{(l)} \rightarrow NaHSe_{(sol)} + B(OC_2H_5)_3 + 3H_{2(g)} \quad (3)$$

In short, NaHSe can be produced in protic solvents such as water and EtOH through appropriate control of the borohydride to selenium ratio. Accordingly, we postulated that we could use both EtOH as redox solvent and water as the electrolyte solvent to remove the formation of undesirable $Na_2B_4O_7$ while benefiting from faster kinetics of highly polar water (R2). In this route, the NaHSe solution was formed in EtOH and was slowly added to the suspension of Sb_2Se_3, NaOH, and Se in water. Although the rate of aqueous reduction of Se is higher, the ethanolic NaHSe is probably the reagent of choice for preparing binary and ternary selenide, as it is not necessary to remove undesirable tetraborate compounds. In the last approach (R3), only EtOH was utilized in both NaHSe and electrolyte reactions. Similar to its sulfide analog, Na_3SbSe_4 is insoluble in EtOH; hence, its reactive precipitation recovery is facilitated through centrifugation and RT vacuum drying which provides a processing advantage over R1 and R2 routes (Centrifugation and supernatant drying at 150 °C). Figure 2 illustrates the various combinations of reagents and solvents used for the synthesis of Na_3SbSe_4 in protic solvents.

The physicochemical properties of the obtained materials were studied by XRD, Raman, and FTIR spectroscopy. Figure 3a shows the diffraction patterns of the as-synthesized Na_3SbSe_4 electrolytes from water (R1), water−ethanol (R2), and ethanol (R3) solvent routes, confirming the formation of the cubic phase of Na_3SbSe_4 (PDF 04-008-2989). The aqueous Na_3SbSe_4 pattern (R1) does not exhibit any crystalline impurities, nor does it rule out the existence of amorphous or nondetectable species in the product. The Raman spectrum of aqueous Na_3SbSe_4 confirms the formation

https://doi.org/10.1021/acs.inorgchem.3c01799
Inorg. Chem. 2023, 62, 17102−17114

of $SbSe_4^{3-}$ polyanions as its stretching modes are observed at 202, 256, and 265 cm^{-1}.[37,53] $SbSe_4^{3-}$ is the building block for cubic Na_3SbSe_4. The peak at 249 cm^{-1} could be assigned either to the Sb−Se stretching mode from the unreacted Sb_2Se_3 precursor or interchain stretching from deposited amorphous selenium.[54,55] As no trace of crystalline Sb_2Se_3 was observed in XRD, we can assume that this Raman peak solely originates from the presence of the unreacted Se precursor. We attribute the incomplete consumption of Se to the reactivity of the tetraborate byproduct in the solution. Klayman and Griffin[47] stated that borax can react with the available NaHSe in the presence of extra Se, as shown in eq 4. This reaction produces sodium diselenide and boric acid (H_3BO_3) byproducts.

$$2NaHSe_{(sol)} + Na_2B_4O_{7(sol)} + 2Se_{(s)} + 5H_2O_{(l)} \rightarrow 2Na_2Se_{2(sol)} + 4H_3BO_{3(sol)} \quad (4)$$

Depletion of NaHSe from this side reaction leads to incomplete conversion and the presence of residual amorphous Se reagent in the final product, as suggested by Raman data. FTIR spectroscopy was utilized to help identify other possible impurities formed in this synthesis approach (Figure S3 and Table S1). The absorbance spectrum of the aqueous sample mainly shows features from boric acid, deposited borax, and other oxidized selenium impurities, confirming the role of borax in diminishing the required NaHSe precursor for electrolyte formation. Due to the similarity of borax and boric acid IR active signals, a quantitative analysis of the impurities' composition seems unreliable, but qualitatively, we can safely assume that most impurities are boric acid.

In the case of the aqueous-ethanolic reaction (R2), we expected to minimize the extent of impurities, esp. borax, present in the final products; however, IR results revealed otherwise. Boric acid IR signals in aqueous-ethanolic Na_3SbSe_4 are stronger than in the aqueous sample, suggesting that the mixing of water and ethanol favors the formation of boric acid. This could be explained based on the fact that triethyl borate can convert to boric acid and ethanol through hydrolysis (eq 5).[47] As a result, the aqueous-ethanolic route might have improved the borax formation judging from a weaker Se Raman peak, but it produces more boric acid and other impurities, that is, $Na_2SbO_{7,}$ simultaneously.

$$B(C_2H_5O)_{3(sol)} + 3H_2O_{(l)} \rightleftharpoons H_3BO_{3(sol)} + 3C_2H_5OH_{(l)} \quad (5)$$

This prompted us to turn our attention to using only EtOH as the reaction medium (R3). First, a 0.5 M ethanolic solution of NaHSe was prepared by adding 10% excess $NaBH_4$ to Se in EtOH which was later used as a NaHSe source for the following experiments. To prepare ethanolic Na_3SbSe_4, stoichiometric quantities of NaHSe solution, Sb_2Se_3, NaOH, and Se and an extra volume of EtOH to adjust the concentration of the product were reacted. The electrolyte was recovered by multiple centrifugations and washing with EtOH and drying the precipitate at RT overnight under vacuum. This obtained sample was denoted as "R3, 1× NaHSe". Additional details on the synthetic conditions are provided in the Experimental Section.

The diffraction pattern of the R3, 1× NaHSe displays the cubic Na_3SbSe_4 with traces of Na_3SbSe_2 secondary phase, while no impurity was observed in the corresponding Raman spectrum (Figure 3a,b). Xiong and co-workers[36] also reported the presence of $NaSbSe_2$ impurities in their solid-state synthesized $Na_3SbSe_{4-x}S_x$ sample which was mainly ascribed to the loss of S and Se during high-temperature solid-state ampule synthesis (650 °C). As the natures of solid-state and solution-phase synthetic approaches are different, we focused on understanding the reaction mechanism more to determine the source of the $NaSbSe_2$ byproduct. As in the mechanism suggested for Na_3SbS_4 in protic solvents,[22,56] we hypothesized that the production of Na_3SbSe_4 in water and ethanol proceeds as follows:

$$Sb_2Se_{3(s)} + HSe^-_{(sol)} + OH^-_{(sol)} \rightarrow Sb_2Se^{2-}_{4(sol)} + H_2O_{(l)} \quad (6)$$

$$Sb_2Se^{2-}_{4(sol)} + 2HSe^-_{(sol)} + OH^-_{(sol)} \rightarrow 2SbSe^{-3}_{3(sol)} + 2H_2O_{(l)} \quad (7)$$

$$2SbSe^{3-}_{3(sol)} + 2Se_{(s)} \rightarrow 2SbSe^{3-}_{4(sol)} \quad (8)$$

An insufficient quantity of HSe^{-1} or OH^- ions in the solution could lead to the low conversion of reagents in eq 7, which ultimately leaves intermediate species such as $Sb_2Se_4^{2-}$ unreacted. The subsequent decomposition of this unstable intermediate led to the formation of $NaSbSe_2$.

$$Na_2Sb_2Se_{4(sol)} \rightarrow 2NaSbSe_{2(s)} \quad (9)$$

The formation of $NaSbSe_2$ can simply be written as shown in eq 10:

$$NaHSe_{(sol)} + Sb_2Se_{3(s)} + NaOH_{(sol)} \rightarrow 2NaSbSe_{2(s)} + H_2O_{(l)} \quad (10)$$

To ensure the availability of HSe^- ions, we added twice the stoichiometric quantity of ethanolic NaHSe solution to repeat the reaction (represented as "R3, 2× NaHSe"), which leads to a phase-pure Na_3SbSe_4, as confirmed by XRD and Raman results. Rietveld refinement of the diffraction pattern was performed by using a crystal structure with space group $I\bar{4}3m$ (Figure S4). The refinement results demonstrate that the recovered electrolyte purely entailed cubic Na_3SbSe_4 with the lattice constant of a = 7.4803 Å consistent with values reported in the literature.[36,37,57] The cubic polymorph in Na_3SbSe_4 typically consists of body-centered cubic sublattice of $SbSe_4$ tetrahedra and Na ions that occupy the octahedral sites.[35] SEM and EDX mapping revealed a powder homogeneously agglomerated in 5−10 μm clusters with appropriate stoichiometry and no segregation among its constituent atoms (Figure S5).

To investigate the thermal stability and potential of residual solvent impurities, TGA was performed on the Na_3SbSe_4 sample recovered from EtOH (Figure 3c). The weight trace and its derivative exhibit three distinct processes at ∼140 °C, ∼235, and ∼307 °C. The gradual weight reduction (<1%) accompanied by a broad peak in the weight derivative signal at ∼140 °C is probably due to the evaporation of ethanol-solvated moieties. Ethanol-complexed chalcogenides are very stable, and typically elevated temperatures relative to their boiling point are required to eliminate all the residuals without altering the compound of interest. We recently showed that a minimum temperature of 300 °C is required to fully purify the Li_2S fabricated through metathesis in EtOH.[58] IR spectra of heat-treated ethanolic Na_3SbSe_4 (Figure S6) confirm the full removal of EtOH-solvated complexes at 200 °C. The slight decline of the TGA scan at ∼235 °C can be attributed to the

https://doi.org/10.1021/acs.inorgchem.3c01799
Inorg. Chem. 2023, 62, 17102−17114

excess Se that has been evaporated, and last, the slow but gradual reduction starting at ~307 °C could imply the onset of the ternary compound decomposition through loss of bonded Se.[59] XRD shows that Na_3SbSe_4, like its sulfide analog, crystallizes to the cubic phase at RT, and additional annealing does not appear to change the broadening or sharpness of the Bragg reflections (Figure 3d). As suggested by the TGA scan, heat treatment above ~300 °C initiates the decomposition of the ternary electrolyte, as traces of $NaSbSe_2$ are evident in the diffraction pattern of the 400 °C sample.

Amine-thiol Synthesis of Na_3SbSe_4. In the previous section, we demonstrated that protic polar solvents such as H_2O and EtOH are suitable media for the synthesis of ternary Na_3SbSe_4 in suspension using $NaBH_4$ and NaOH as reducing and basic reagents, respectively. However, solvents that could fully dissolve all reagents and drive the reaction to completion without any other reagents would be more desirable, as they simplify the synthesis process and enable a similar yield ultimately. Moreover, this approach can produce homogeneous SSE solutions that could be further extended in the production of composite cathodes. This inspired us to investigate other wet-chemistry approaches for the synthesis of selenide inorganic materials. Specifically, simple amines like 1,2-ethylene diamine (EDA) have been used extensively to produce thermoelectric selenides such as Cu_3SbSe_4 and its doped derivatives at reflux conditions.[60,61] We employed a similar approach, in which elemental Na, Se, and Sb_2Se_3 with the stoichiometry shown in eq 11 were dispersed in EDA and examined the impact of different reaction temperatures in the formation of the desired selenide. As Na_3SbSe_4 is soluble in EDA within the concentration range used, the supernatant was evaporated at 150 °C in an Ar atmosphere to obtain the SSE powder.

$$6Na + Sb_2Se_3 + 5Se \rightarrow 2Na_3SbSe_4 \quad (11)$$

Figure 4 exhibits the XRD and Raman spectra of samples obtained from the EDA synthetic route conducted at 90 and

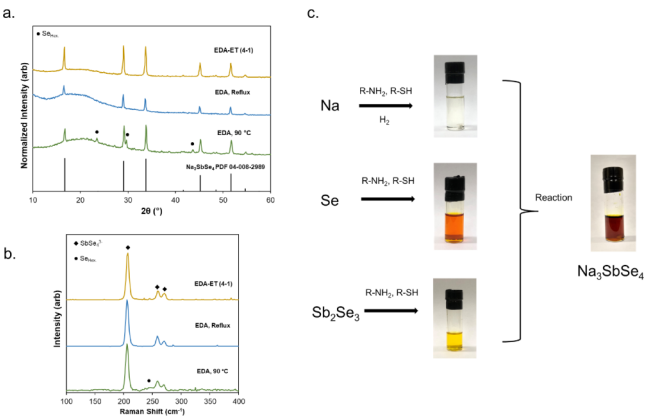

Figure 4. (a) XRD and (b) Raman spectra of the electrolyte derived from EDA and EDA-ET (4−1) solutions. (c) Schematics of amine-thiol formation of Na_3SbSe_4.

130 °C (Reflux). The sample at 90 °C shows significant traces of unreacted hexagonal Se mostly due to insufficient dissolution. In contrast, conducting the reaction under reflux forms phase-pure Na_3SbSe_4 SSE in nearly 60% yield. The diffraction patterns are not corrected for the background diffraction to help identify the crystallinity difference. Amines such as 1,2-ethylene diamine and oleyamine have relatively weak reducing abilities, which hinder the dissolution of large Se quantities at mild conditions ultimately requiring high temperatures.[62] Even though the collected product from the reflux is highly pure, unfavorable reflux requirements such as a high-temperature reaction and relatively more complicated equipment used render this method less amenable for large-scale productions compared to the alcohol-mediated approach.

Improving amine ($R\text{-}NH_2$) dissolution of Se through the addition of alkali borohydrides such as $NaBH_4$ and KBH_4 has been successful in synthesizing binary selenides,[63,64] but considering the high solubility of ternary Na_3SbSe_4, the addition of boron and its derivatives adds to the complexity of product purity. Alternatively, several research groups[62,65] introduced alkylthiol (R-SH) reducing agents to dissolve Se in large concentrations through a series of amine-thiol protonation and deprotonation, which produces ammonium ions and alkyl disulfide, a thiolate species. The resulting thiolate remains in solution and opens the Se ring through nucleophilic attack, while the ammonium further reacts with reduced Se to form an ammonium complex of Se, $[(Se^{2-})(R\text{-}NH_3^+)_2]$. Further studies by the Agarwal group[66] showed that the monoamine and diamine solvents combined with monothiols could lead to different polyselenide complexes.

Nevertheless, this solvated Se complex remains soluble in an amine-thiol mixture and can be utilized in conjunction with other precursors to form other selenides. The combination of amine-thiol solvents has been developed to dissolve bulk metals, metal oxides, and chalcogenides, which are mainly applied in the solution processing of inorganic semiconductors. The metal thiolates formed as a result can be used without the need for purification or separation.[40,62,65,67] Besides, Lee et al.[38] have recently introduced the use of an amine-thiol mixture as an alkahest solution system to produce various Li/Na sulfides SSEs (Li_6PS_5Cl, $L_{10}GeP_2S_{12}$, and $Na_{11}Sn_2PS_{12}$). However, the formation of residual carbon impurities during solvent removal and powder recovery hinders their utilization in Na-based SSEs.

Inspired by these studies, we explored the addition of ethanethiol (ET), the most volatile and lightest available thiol, to EDA. Small amounts of Sb_2Se_3, Se, and Na were all dissolved very quickly in an EDA-ET (4:1, v/v) mixture, yielding yellow, light orange, and clear solutions, respectively (Figure 4c). Notably, the dissolution of elemental Na involved slight gas evolution. Zhao et al.[67] identified H_2 evolution and formation of metallic thiolates during the dissolution of In and Cu bulk metals in hexylamine-1,2 ethanedithiol (10:1, v/v) solution. Accordingly, we can assume that Na follows a similar dissolution chemistry, forming a mix of thiolates and H_2 gas. The Na_3SbSe_4 reaction was conducted by adding stoichiometric quantities of precursor powders (0.17 M wrt to Na_3SbSe_4) to 10 mL of EDA-ET (4:1, v/v). After the initial fast dissolution, the solution turned dark red. The solution was centrifuged to discard any undissolved species, and the brown powder was recovered by evaporation of the solvents at 150 °C in Ar. The obtained powder was highly crystalline, and the diffraction pattern matched very well with the cubic phase of Na_3SbSe_4, while Raman confirmed the formation of constituent tetrahedral $SbSe_4$ units with no apparent impurity (Figure 4a, b).

FTIR spectra (Figure S7) of Na_3SbSe_4 derived from the EDA-ET mixture evaporated at 150 °C lacked any solvent features, specifically ν(C−H) and ν(N−H) stretching bands at

https://doi.org/10.1021/acs.inorgchem.3c01799
Inorg. Chem. 2023, 62, 17102−17114

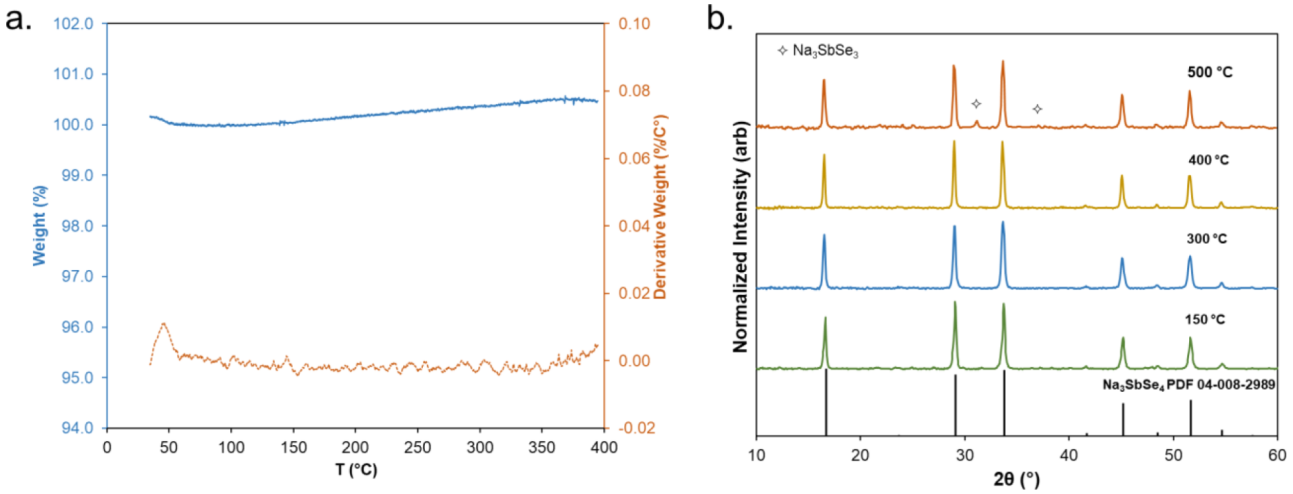

Figure 5. (a) TGA curves of Na_3SbSe_4 powders derived from EDA-ET (4−1) solution at 150°C and (b) XRD patterns of Na_3SbSe_4 were derived from EDA-ET (4−1) solvents and annealed at different temperatures.

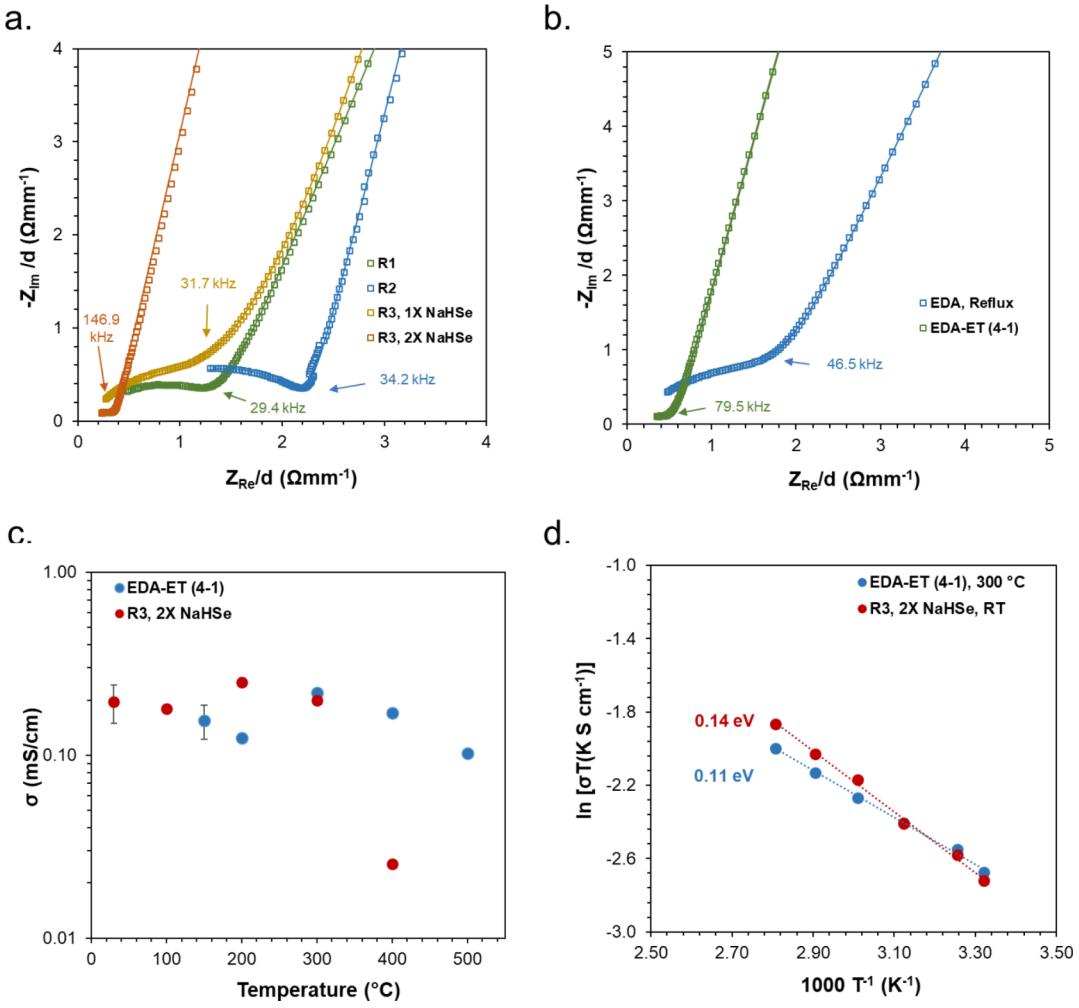

Figure 6. Nyquist plots of Na_3SbSe_4 recovered from (a) alcohol-mediated and (b) amine-thiol approaches. (c) Ionic conductivity of the corresponding Na_3SbSe_4 at various heat-treatment temperatures. (d) Arrhenius plots of Na_3SbSe_4 recovered from EtOH (R3, 2× NaHSe) and EDA-ET (heat-treated at 300 °C).

2750−3350 cm^{-1}. Additionally, thiol signatures such as C−S stretching (653 cm^{-1}), S−H bending mode (~870 cm^{-1}), and slight ν(S−H) stretching band (2500−2600 cm^{-1}) observed in ET solvent are absent.[38,68,69] This indicates the low energetics needed to achieve recovery of the phase-pure selenide.

TGA of Na_3SbSe_4 derived from EDA-ET displays a very stable phase, further verifying the removal of solvents as

https://doi.org/10.1021/acs.inorgchem.3c01799
Inorg. Chem. 2023, 62, 17102−17114

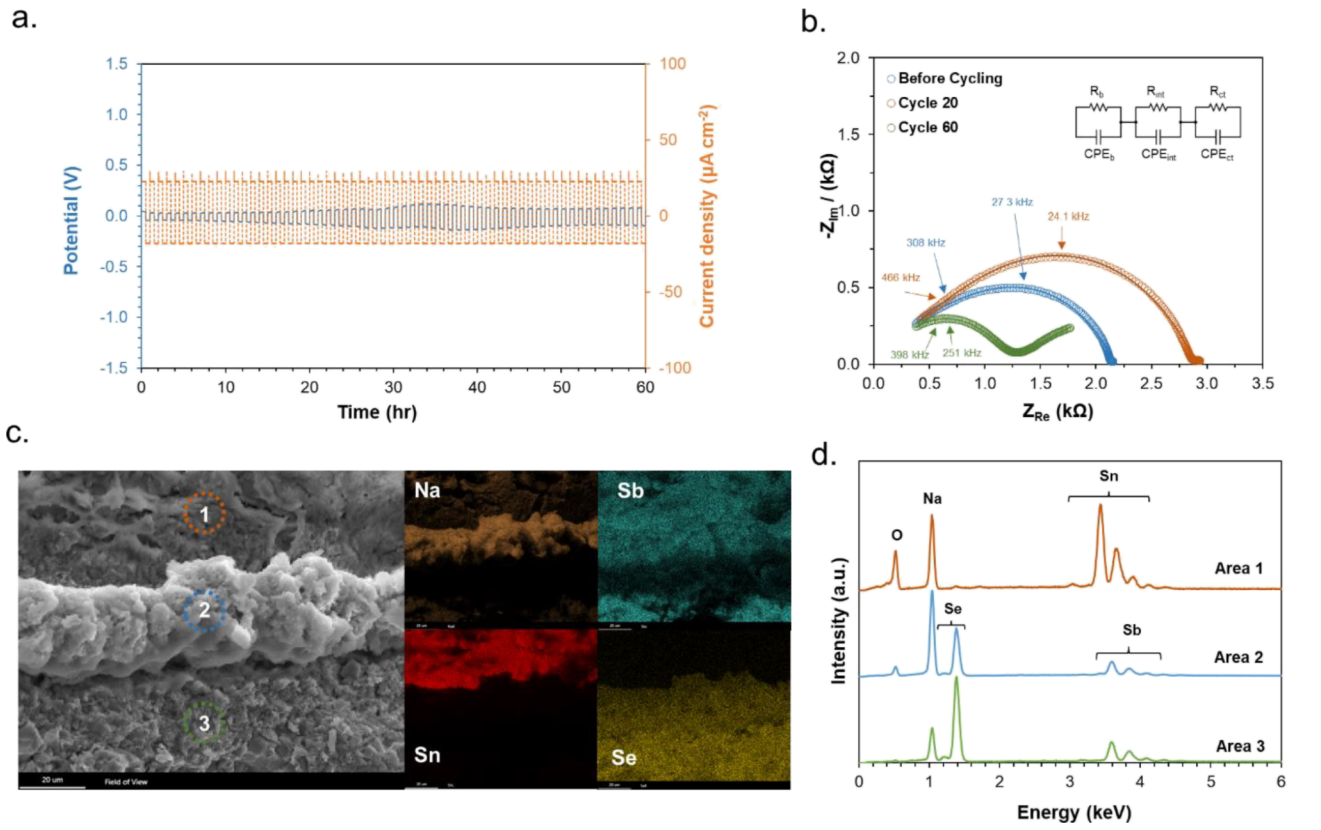

Figure 7. (a) Symmetric cell cycling of $Na_{15}Sn_4|Na_3SbSe_4|Na_{15}Sn_4$ cell with a current density of 0.02 mA cm^{-2} at 60 °C, (b) Nyquist plots and fitted spectra of the cell before and after cycling for 20 and 60 h, (c) cross-sectional SEM image of the symmetric pellet after 60 h of stripping/plating with corresponding EDX maps of constituent elements, and (d) EDX spectra of various areas denoted on the SEM cross-section image.

suggested by FTIR results (Figure 5a). The different trend seen in the thermal analysis of SSE recovered from EDA-ET in comparison with the ethanolic sample highlights the difference in the underlying mechanisms of the two approaches with different intermediate species and kinetics. For instance, unlike the ethanolic sample, there is no trace of excess unreacted Se in the 200−300 °C range. Further heat treatment of Na_3SbSe_4 was performed for consistency with the ethanolic study. As indicated in the TGA investigation, SSE derived from amine-thiol is stable until 400 °C, even though a small trace of Se-deficient Na_3SbSe_3 is noticeable in XRD patterns. The intermediate reflection becomes significantly larger at 500 °C, indicating the onset of decomposition. The Rietveld refinement (Figure S8) of the sample heat-treated at 300 °C mainly consisted of cubic Na_3SbSe_4 with a lattice constant of 7.4866 Å similar to the ethanolic sample. The weight fraction of Na_3SbSe_3 is around 0.03%. Morphology investigation shows similar inhomogeneous microstructures with a uniform elemental distribution (Figure S9). It is notable that the SSE from the amine-thiol route is a light brown powder unlike the ethanolic products, which have a darker shade, presumably due to the presence of absorbed Se (Figure S6). In the following section, the electrochemical performance of as-synthesized Na_3SbSe_4 obtained from two synthetic approaches will be discussed.

Na_3SbSe_4 Electrochemical Performance and Air Stability. Na^+ conductivity and activation barrier were evaluated through temperature-dependent impedance spectroscopy. The electrolyte pellets were formed by isostatic cold pressing at a pressure of 270 MPa at room temperature with no additional sintering steps. As demonstrated in Figure 6a, b, the EIS spectra of recovered electrolytes for all samples consist of a high-frequency repressed semicircle and a blocking arc at mid to low frequency, which are attributed to Na^+ diffusion contribution and the electrode polarization, respectively. The pellet resistances were derived by fitting the impedance spectra to an equivalent circuit consisting of a constant phase element in parallel with a resistor which is in series with another constant phase element for R1, R3 2× NaHSe, and EDA-ET (4-1) samples. In the case of R2 and R3 1× NaHSe and EDA Reflux data, another RC element is considered to explain the grain boundary contribution and improve the fitting (Table S2). The ionic conductivity is derived from $\sigma = \frac{l}{RA}$, in which l, A, and R are pellet thickness, surface area, and calculated resistance from equivalent circuit fitting.

Figure 6c presents the ionic conductivity of samples recovered from ethanol (R3, 2× NaHSe) and EDA-ET (4−1) solvents as a function of the heat-treatment temperature. The ionic conductivity obtained from both routes was $\sigma_{Na+} \sim 0.2$ mS cm^{-1}, and the results were weakly dependent on the annealing temperature owing to its high crystallinity at low temperatures. Conductivity declined for samples annealed at temperature >300 °C, particularly in the ethanol system, which was attributed to the low conductivity of the $NaSbSe_2$ phase. The activation energy was calculated based on the Arrhenius equation. A smaller value of 0.11−0.14 eV in comparison with activation energies reported from Na_3SbSe_4 synthesized from the solid-state routes (Table S3) was realized in our work, which could be attributed to different data acquisition protocols and experimental conditions of various research

https://doi.org/10.1021/acs.inorgchem.3c01799
Inorg. Chem. 2023, 62, 17102−17114

Table 1. Summary of Solution Derived Na_3SbSe_4 Experimental Parameters and Their Performance

sample	H_2O (v %)	EtOH (v %)	NaHSe/Na_3SbSe_4 molar ratio	heat-treatment (°C)	products	σ (mS cm^{-1})
R1	100	0	3/2	150	**Na_3SbSe_4**, Sb_2Se_3, H_3BO_3	0.056
R2	75	25	3/2	150	**Na_3SbSe_4**, Sb_2Se_3, H_3BO_3	0.038
R3, 1× NaHSe	0	100	3/2	RT	**Na_3SbSe_4**, $NaSbSe_2$	0.030
R3, 2× NaHSe	0	100	3	RT	**Na_3SbSe_4**	0.195
R3, 2× NaHSe, 200 °C	0	100	3	200	**Na_3SbSe_4**	0.250
sample	EDA (v %)	ET (v %)		heat-treatment (°C)	products	σ (mS cm^{-1})
EDA, 90 °C	100	0		150	**Na_3SbSe_4**, Se	
EDA, Reflux	100	0		150	**Na_3SbSe_4**	0.051
EDA-ET (4−1)	80	20		150	**Na_3SbSe_4**, Na_3SbSe_3 (trace)	0.123
EDA-ET (4−1), 300 °C	80	20		300	**Na_3SbSe_4**, Na_3SbSe_3 (trace)	0.175

groups. Temperature-dependent Nyquist plots are presented in Figure S10. DC polarization measurements (Figure S11) of Na_3SbSe_4 powder recovered from both systems show an inconsequential electronic conductivity of 1.4−1.6 × 10^{-6} mS cm^{-1}, which is 5 orders of magnitude lower than the recorded ionic conductivity characteristics of solid-state superionic conductors.

To realize all-solid-state sodium batteries with high energy density and capacity, Na metal has been proposed as an anode candidate owing to its high theoretical capacity (1165.8 mAh g^{-1}) and low electrochemical potential (−2.7 V vs SHE).[70] However, Na metal is highly reductive and incompatible with most solid-state electrolytes such as chalcogenides, resulting in inhomogeneous plating/stripping and dendrite penetration. As a solution, Na-based alloys like Na−Sn have been extensively studied as alternatives to improve the anode-electrolyte interfacial stability.[8,71,72] As a proof of concept, we investigated the chemical and electrochemical stability of Na_3SbSe_4 with $Na_{15}Sn_4$ in a symmetric cell setup. For this study, $Na_{15}Sn_4$ was prepared through ball-milling, and its formation was confirmed by XRD measurements (Figure S12). The XRD pattern shows traces of unreacted Na present in the final electrode composition.

To better understand the chemical stability of $Na_{15}Sn_4$ against Na_3SbSe_4, the symmetric cell was monitored with EIS at an OCV of 0 V at 60 °C without biasing (Figure S13a and Table S3). The Nyquist plots were fit to an equivalent circuit (inset) that accounts for the electrolyte bulk resistance R_b, solid-electrolyte interface (SEI) resistance R_{int}, and the electrolyte-electrode charge transfer resistance R_{ct}.[73] The low-frequency electrode contribution was quite weak and did not produce reliable fittings for impedance data due to instrumental frequency limitations. Figure S13b shows the extracted bulk and interface area-specific resistance (ASR). It was found that $Na_{15}Sn_4$ can form a stable interface with the selenide after 2 h. Here, the interface resistance increases slightly, while the bulk resistance initially has an abrupt rise, most likely because of selenide reduction and subsequent SEI formation. Once the SEI is fully formed, the overall cell resistance starts to decline.

Figure 7a shows the voltage−time profile of $Na_{15}Sn_4$ stripping/plating at a current density of 0.02 mA cm^{-2} at 60 °C after aging for 2 h. The initial polarization voltage was approximately 43 mV and gradually increased within the first ∼36 h of cycling and started to stabilize afterward. The overpotential remained relatively small and stable after 60 h, indicating the presence of a robust SEI layer. EIS was used to monitor the evolution of cell resistance before and after cycling for 20 and 60 h (Figure 7b). The fitting parameters and corresponding capacitances are displayed in Table S3. The increase in the total resistance of the cell is consistent with the constant, yet slow, rise in the potential of the symmetric cell, but the contribution from the individual resistances varies through different cycles.

Cross-sectional SEM and EDX mapping were conducted before (Figure S14) and after 60 cycles (Figure 7c) to probe the evolution of the $Na_{15}Sn_4$−Na_3SbSe_4 interface. A 20−30 μm interlayer was observed where it separated the electrode−electrolyte interface into 3 areas. To further complement the mapping results, individual EDX spectra were collected in areas 1, 2, and 3 which correspond to the electrode, SEI layer, and electrolyte, respectively (Figure 7d). Due to the inhomogeneous surface of the cross-sectional cut and the proximity of Sb and Sn peaks, the gradient in elemental concentration observed in Sb mapping is quite unreliable. However, we can clearly observe the presence of reduced species containing Na, Sb, and Se in the SEI layer likely to originate from Na_3Sb and Na_2Se compounds based on similar chemistry of Na_3SbSe_4 to Na_3PSe_4. Tian et al.[8] predicted that Na−P and Na_2Se materials could be the decomposition products of Na_3PSe_4 cycled against Na anodes using DFT calculations. The formation of a relatively thick SEI containing the reduced species correlates well with the total resistance increase observed after cycling. Further post-mortem cell experiments such as X-ray photon spectroscopy (XPS) are necessary to elucidate the nature of chemical species formed in the $Na_{15}Sn_4$|Na_3SbSe_4 interface, but this study suggests that $Na_{15}Sn_4$ is a suitable candidate to be coupled with the selenide electrolyte for a long-term Na all-solid-state battery.

To assess the air stability of ternary selenide electrolytes in an ambient atmosphere, a pellet of ethanolic Na_3SbSe_4 was exposed to air with RH ∼ 40% for 1 day. The XRD patterns, IR spectra, and ionic transport of the pellet before and after exposure were measured. As displayed in Figure S15, the crystallinity of the air-exposed sample slightly diminishes with minimal peak broadening compared to the pristine sample, while the overall crystalline structure is retained with no apparent presence of new phases. The peak broadening could be due to the presence of adsorbed moisture.[74] This is verified through IR spectroscopy as the absorbances of oxygenated and OH-bonded species are intensified after exposure to air. Therefore, the slight reduction in conductivity is due to an infinitesimal decrease in crystallinity and absorption of moisture on the electrolyte surface.

https://doi.org/10.1021/acs.inorgchem.3c01799
Inorg. Chem. 2023, 62, 17102−17114

Table 1 summarizes the experimental conditions for the liquid synthesis of Na_3SbSe_4 samples, resulting in purity and electrochemical performance. Among protic solvents, ethanolic Na_3SbSe_4 with excess NaHSe concentration (R3, 2× NaHSe) at RT produces a high conductivity of 0.195 mS cm^{-1}, which is ∼4 times larger than aqueous Na_3SbSe_4. Boric acid and borax impurities are the main reasons for the low conductivity achieved from aqueous electrolytes. In the case of amine-thiol synthesis, the sample recovered from mixed solvent shows a higher conductivity that is mainly attributed to better crystallinity obtained through a thermodynamically favorable reaction facilitated by the addition of ethanethiol.

CONCLUSIONS

In summary, this study illustrates two novel liquid-based approaches for the synthesis of air-stable Na_3SbSe_4 solid-state electrolytes. First, binary Sb_2Se_3 was fabricated through a metathesis route and utilized as a precursor in subsequent Na_3SbSe_4 formation. Amorphous Sb_2Se_3 was crystallized through mild heat treatment and used as synthesized with no apparent impurities in the electrolyte reactions. Next, alcohol-mediated redox (suspension-based) and amine-thiol (solution-based) approaches were used to successfully synthesize Na_3SbSe_4 in EtOH and EDA-ET cosolvent mixtures. The electrolyte recovered from the ethanolic suspension without any postreaction treatment has a significant ionic conductivity of 0.2 mS cm^{-1} and activation energy of 0.14 eV, which are slightly lower than previous reports of the synthesized Na_3SbSe_4 (Table S2). A similar electrochemical performance is achieved from Na_3SbSe_4 from the amine-thiol route recovered with mild heat treatment. The ethanol route requires the use of excess NaHSe to drive the reaction to completion, but benefits from reactive precipitation that enables product recovery at room temperature. In the alkahest approach, the addition of ET enhanced reactivity and the electrolyte is recovered by solvent evaporation and annealing at 150 °C. We also showed that $Na_{15}Sn_4$ is a compatible anode that could be utilized with Na_3SbSe_4 in Na all-solid-state batteries. This study has provided key insights into the formation mechanism and expands routes for the solution synthesis of selenide compounds of interest for Na all-solid-state batteries as well as other applications.

ASSOCIATED CONTENT

Supporting Information

The Supporting Information is available free of charge at https://pubs.acs.org/doi/10.1021/acs.inorgchem.3c01799.

XRD and EDX data of Sb_2Se_3 products; FTIR data and table of associate peaks, SEM and EDX mapping, and XRD Rietveld refinement of Na_3SbSe_4 recovered from alcohol-mediated and amin-thiol approaches; temperature-dependent Nyquist plots and chronoamperometry plots of Na_3SbSe_4; XRD patterns of $Na_{15}Sn_4$; EIS spectra and SEM and EDX mapping of a $Na_{15}Sn_4$ symmetric cell; and XRD, FTIR, and EIS data of pristine and air-exposed ethanolic Na_3SbSe_4 (PDF)

AUTHOR INFORMATION

Corresponding Author

Colin A. Wolden − *Chemical and Biological Engineering, Colorado School of Mines, Golden, Colorado 80401, United States;* orcid.org/0000-0001-6576-048X; Email: cwolden@mines.edu

Authors

Saeed Ahmadi Vaselabadi − *Chemical and Biological Engineering, Colorado School of Mines, Golden, Colorado 80401, United States*

Katie Palmer − *Chemical Engineering, Rose-Hulman Institute of Technology, Terre Haute, Indiana 47803-3999, United States;* orcid.org/0000-0001-9841-9587

William H. Smith − *Chemical and Biological Engineering, Colorado School of Mines, Golden, Colorado 80401, United States*

Complete contact information is available at: https://pubs.acs.org/10.1021/acs.inorgchem.3c01799

Author Contributions

The manuscript was written through contributions of all authors. All authors have given approval to the final version of the manuscript. S.V. and C.W. conceived the initial idea and designed the experiments. S.V., K.P., and W.S. performed the experiments and analyzed the data. S.V. and C.W. drafted the article. All authors commented on the manuscript.

Notes

The authors declare no competing financial interest.

ACKNOWLEDGMENTS

This work was supported by the National Science Foundation through Awards 1825470 and 2219184, and the Colorado Office of Economic Development and International Trade. In addition, Katie Palmer was supported through the National Science Foundation Award REU 1950924.

REFERENCES

(1) Riha, S. C.; Parkinson, B. A.; Prieto, A. L. Solution-Based Synthesis and Characterization of Cu2ZnSnS4 Nanocrystals. *J. Am. Chem. Soc.* **2009**, *131* (34), 12054−12055.

(2) Lafond, A.; Guillot-Deudon, C.; Vidal, J.; Paris, M.; La, C.; Jobic, S. Substitution of Li for Cu in Cu2ZnSnS4: Toward Wide Band Gap Absorbers with Low Cation Disorder for Thin Film Solar Cells. *Inorg. Chem.* **2017**, *56* (5), 2712−2721.

(3) Sootsman, J. R.; Chung, D. Y.; Kanatzidis, M. G. New and Old Concepts in Thermoelectric Materials. *Angew. Chem., Int. Ed.* **2009**, *48* (46), 8616−8639.

(4) Kanatzidis, M. G. Discovery-Synthesis, Design, and Prediction of Chalcogenide Phases. *Inorg. Chem.* **2017**, *56* (6), 3158−3173.

(5) Jia, H.; Peng, L.; Yu, C.; Dong, L.; Cheng, S.; Xie, J. Chalcogenide-Based Inorganic Sodium Solid Electrolytes. *J. Mater. Chem. A* **2021**, *9*, 5134−5148.

(6) Ellis, B. L.; Nazar, L. F. Sodium and Sodium-Ion Energy Storage Batteries. *Curr. Opin Solid State Mater. Sci.* **2012**, *16* (4), 168−177.

(7) Thangadurai, V.; Chen, B. Solid Li- and Na-Ion Electrolytes for Next Generation Rechargeable Batteries. *Chem. Mater.* **2022**, *34* (15), 6637−6658.

(8) Tian, Y.; Shi, T.; Richards, W. D.; Li, J.; Kim, J. C.; Bo, S.-H.; Ceder, G. Compatibility Issues between Electrodes and Electrolytes in Solid-State Batteries. *Energy Environ. Sci.* **2017**, *10* (5), 1150−1166.

(9) Hou, D.; Xia, D.; Gabriel, E.; Russell, J. A.; Graff, K.; Ren, Y.; Sun, C.; Lin, F.; Liu, Y.; Xiong, H. Spatial and Temporal Analysis of Sodium-Ion Batteries. *ACS Energy Lett.* **2021**, *6* (11), 4023−4054.

(10) Yang, H.-L.; Zhang, B.-W.; Konstantinov, K.; Wang, Y.-X.; Liu, H.-K.; Dou, S.-X. Progress and Challenges for All-Solid-State Sodium Batteries. *Adv. Energy Sustainability Res.* **2021**, *2* (2), No. 2000057.

(11) Tang, B.; Yu, X.; Gao, Y.; Bo, S. H.; Zhou, Z. Positioning Solid-State Sodium Batteries in Future Transportation and Energy Storage. *Sci. Bull.* **2022**, *67* (21), 2149−2153.
(12) Famprikis, T.; Canepa, P.; Dawson, J. A.; Islam, M. S.; Masquelier, C. Fundamentals of Inorganic Solid-State Electrolytes for Batteries. *Nat. Mater.* **2019**, *18* (12), 1278−1291.
(13) Bo, S. H.; Wang, Y.; Kim, J. C.; Richards, W. D.; Ceder, G. Computational and Experimental Investigations of Na-Ion Conduction in Cubic Na3PSe4. *Chem. Mater.* **2016**, *28* (1), 252−258.
(14) Zhao, C.; Liu, L.; Qi, X.; Lu, Y.; Wu, F.; Zhao, J.; Yu, Y.; Hu, Y. S.; Chen, L. Solid-State Sodium Batteries. *Adv. Energy Mater.* **2018**, *8* (17), No. 04225.
(15) Han, S.; Seo, J. Y.; Park, W. B.; Ikhe, A. B.; Choi, S. Y.; Han, S. C.; Sohn, K.-S.; Pyo, M. Vacancy-Controlled Quaternary Sulfide Na3−xZn1−xGa1+xS4 with Improved Ionic Conductivity and Aqueous Stability. *J. Mater. Chem. A* **2022**, *10* (47), 25039−25046.
(16) Jansen, M.; Henseler, U. Synthesis, Structure Determination, and Ionic Conductivity of Sodium Tetrathiophosphate. *J. Solid State Chem.* **1992**, *99* (1), 110−119.
(17) Hayashi, A.; Noi, K.; Sakuda, A.; Tatsumisago, M. Superionic Glass-Ceramic Electrolytes for Room-Temperature Rechargeable Sodium Batteries. *Nat. Commun.* **20123**, 2−6.
(18) Banerjee, A.; Park, K. H.; Heo, J. W.; Nam, Y. J.; Moon, C. K.; Oh, S. M.; Hong, S.-T. T.; Jung, Y. S. Na3SbS4: A Solution Processable Sodium Superionic Conductor for All-Solid-State Sodium-Ion Batteries. *Angew., Chem., Int. Ed.* **2016**, *55* (33), 9634−9638.
(19) Zhang, L.; Zhang, D.; Yang, K.; Yan, X.; Wang, L.; Mi, J.; Xu, B.; Li, Y. Vacancy-Contained Tetragonal Na3SbS4 Superionic Conductor. *Adv. Sci.* **2016**, *3* (10), No. 1600089.
(20) Zhang, D.; Cao, X.; Xu, D.; Wang, N.; Yu, C.; Hu, W.; Yan, X.; Mi, J.; Wen, B.; Wang, L.; Zhang, L. Synthesis of Cubic Na3SbS4 Solid Electrolyte with Enhanced Ion Transport for All-Solid-State Sodium-Ion Batteries. *Electrochim. Acta* **2018**, *259*, 100−109.
(21) Wang, H.; Chen, Y.; Hood, Z. D.; Sahu, G.; Pandian, A. S.; Keum, J. K.; An, K.; Liang, C. An Air-Stable Na3SbS4 Superionic Conductor Prepared by a Rapid and Economic Synthetic Procedure. *Angew. Chem., Int. Ed.* **2016**, *55* (30), 8551−8555.
(22) Vaselabadi, S. A.; Smith, W. H.; Wolden, C. A. Solution Synthesis of Sb2S3 and Na3SbS4 Solid-State Electrolyte. *J. Electrochem. Soc.* **2021**, *168* (11), 110533.
(23) Zhang, Z.; Ramos, E.; Lalère, F.; Assoud, A.; Kaup, K.; Hartman, P.; Nazar, L. F. Na11Sn2PS12: A New Solid State Sodium Superionic Conductor. *Energy Environ. Sci.* **2018**, *11* (1), 87−93.
(24) Duchardt, M.; Ruschewitz, U.; Adams, S.; Dehnen, S.; Roling, B. Vacancy-Controlled Na+ Superion Conduction in Na11Sn2PS12. *Angew. Chem., Int.l Ed.* **2018**, *57* (5), 1351−1355.
(25) Chu, I.-H.; Kompella, C. S.; Nguyen, H.; Zhu, Z.; Hy, S.; Deng, Z.; Meng, Y. S.; Ong, S. P. Room-Temperature All-Solid-State Rechargeable Sodium-Ion Batteries with a Cl-Doped Na3PS4 Superionic Conductor. *Sci. Rep.* **2016**, *6* (1), 33733.
(26) Yu, Z.; Shang, S. L.; Seo, J. H.; Wang, D.; Luo, X.; Huang, Q.; Chen, S.; Lu, J.; Li, X.; Liu, Z. K.; Wang, D. Exceptionally High Ionic Conductivity in Na3P0. 62As0.38S4 with Improved Moisture Stability for Solid-State Sodium-Ion Batteries. *Adv. Mater.* **2017**, *29* (16), 6.
(27) Moon, C. K.; Lee, H. J.; Park, K. H.; Kwak, H.; Heo, J. W.; Choi, K.; Yang, H.; Kim, M. S.; Hong, S. T.; Lee, J. H.; Jung, Y. S. Vacancy-Driven Na+ Superionic Conduction in New Ca-Doped Na3PS4 for All-Solid-State Na-Ion Batteries. *ACS Energy Lett.* **2018**, *3* (10), 2504−2512.
(28) Hayashi, A.; Masuzawa, N.; Yubuchi, S.; Tsuji, F.; Hotehama, C.; Sakuda, A.; Tatsumisago, M. A Sodium-Ion Sulfide Solid Electrolyte with Unprecedented Conductivity at Room Temperature. *Nat. Commun.* **2019**, *10* (1), No. 503693.
(29) Fuchs, T.; Culver, S. P.; Till, P.; Zeier, W. G. Defect-Mediated Conductivity Enhancements in Na3- XPn1- XWxS4 (Pn = P, Sb) Using Aliovalent Substitutions. *ACS Energy Lett.* **2020**, *5* (1), 146−151.
(30) Pearson, R. G. Absolute Electronegativity and Absolute Hardness of Lewis Acids and Bases. *J. Am. Chem. Soc.* **1985**, *107* (24), 6801−6806.
(31) Bo, S. H.; Wang, Y.; Kim, J. C.; Richards, W. D.; Ceder, G. Computational and Experimental Investigations of Na-Ion Conduction in Cubic Na3PSe4. *Chem. Mater.* **2016**, *28* (1), 252−258.
(32) Zhang, L.; Yang, K.; Mi, J.; Lu, L.; Zhao, L.; Wang, L.; Li, Y.; Zeng, H. Na3PSe4: A Novel Chalcogenide Solid Electrolyte with High Ionic Conductivity. *Adv. Energy Mater.* **2015**, *5* (24), 2−6.
(33) Bo, S. H.; Wang, Y.; Ceder, G. Structural and Na-Ion Conduction Characteristics of Na3PS: XSe4- x. *J. Mater. Chem. A* **2016**, *4* (23), 9044−9053.
(34) Krauskopf, T.; Pompe, C.; Kraft, M. A.; Zeier, W. G. Influence of Lattice Dynamics on Na+ Transport in the Solid Electrolyte Na3PS4-XSex. *Chem. Mater.* **2017**, *29* (20), 8859−8869.
(35) Till, P.; Agne, M. T.; Kraft, M. A.; Courty, M.; Famprikis, T.; Ghidiu, M.; Krauskopf, T.; Masquelier, C.; Zeier, W. G. Two-Dimensional Substitution Series Na3P1−XSbxS4−YSey: Beyond Static Description of Structural Bottlenecks for Na + Transport. *Chem. Mater.* **2022**, *34* (5), 2410−2421.
(36) Xiong, S.; Liu, Z.; Rong, H.; Wang, H.; McDaniel, M.; Chen, H. Na3SbSe4-XSx as Sodium Superionic Conductors. *Sci. Rep.* **2018**, *8* (1), 2−8.
(37) Wang, N.; Yang, K.; Zhang, L.; Yan, X.; Wang, L.; Xu, B. Improvement in Ion Transport in Na3PSe4−Na3SbSe4 by Sb Substitution. *J. Mater. Sci.* **2018**, *53* (3), 1987−1994.
(38) Lee, J. E.; Park, K. H.; Kim, J. C.; Wi, T. U.; Ha, A. R.; Song, Y. B.; Oh, D. Y.; Woo, J.; Kweon, S. H.; Yeom, S. J.; Cho, W.; Kim, K. S.; Lee, H. W.; Kwak, S. K.; Jung, Y. S. Universal Solution Synthesis of Sulfide Solid Electrolytes Using Alkahest for All-Solid-State Batteries. *Adv. Mater.* **2022**, *2200083*, 1−11.
(39) Miura, A.; Rosero-Navarro, N. C.; Sakuda, A.; Tadanaga, K.; Phuc, N. H. H.; Matsuda, A.; Machida, N.; Hayashi, A.; Tatsumisago, M. Liquid-Phase Syntheses of Sulfide Electrolytes for All-Solid-State Lithium Battery. *Nat. Rev. Chem.* **2019**, *3* (3), 189−198.
(40) Webber, D. H.; Brutchey, R. L. Alkahest for V2VI3 Chalcogenides: Dissolution of Nine Bulk Semiconductors in a Diamine-Dithiol Solvent Mixture. *J. Am. Chem. Soc.* **2013**, *135* (42), 15722−15725.
(41) Yang, W.; Zhang, X.; Tilley, S. D. Emerging Binary Chalcogenide Light Absorbers: Material Specific Promises and Challenges. *Chem. Mater.* **2021**, *33* (10), 3467−3489.
(42) Chen, S.; Liu, T.; Zheng, Z.; Ishaq, M.; Liang, G.; Fan, P.; Chen, T.; Tang, J. Recent Progress and Perspectives on Sb2Se3-Based Photocathodes for Solar Hydrogen Production via Photoelectrochemical Water Splitting. *J. Energy Chem.* **2022**, *67*, 508−523.
(43) Ge, P.; Cao, X.; Hou, H.; Li, S.; Ji, X. Rodlike Sb2Se3 Wrapped with Carbon: The Exploring of Electrochemical Properties in Sodium-Ion Batteries. *ACS Appl. Mater. Interfaces* **2017**, *9* (40), 34979−34989.
(44) Guo, L.; Cao, L.; Huang, J.; Li, J.; Kajiyoshi, K.; He, J.; Qi, H. Guiding Fabrication of Continuous Carbon-Confined Sb2Se3 Nanoparticle Structure for Durable Potassium-Storage Performance. *ACS Appl. Energy Mater.* **2021**, *4* (9), 10391−10403.
(45) Luo, W.; Calas, A.; Tang, C.; Li, F.; Zhou, L.; Mai, L. Ultralong Sb2Se3 Nanowire-Based Free-Standing Membrane Anode for Lithium/Sodium Ion Batteries. *ACS Appl. Mater. Interfaces* **2016**, *8* (51), 35219−35226.
(46) MilliporeSigma. *Antimony(III) selenide*. https://www.sigmaaldrich.com/US/en/product/aldrich/401196.
(47) Klayman, D. L.; Griffin, T. S. Reaction of Selenium with Sodium Borohydride in Protic Solvents. A Facile Method for the Introduction of Selenium into Organic Molecules. *J. Am. Chem. Soc.* **1973**, *95* (1), 197−199.
(48) Vidyadharan, D. M.; Pullanjiyot, N.; Ninnora Meethal, B.; Kanakkillam, S. S.; Sadasivan, S.; Swaminathan, S. Highly Stable Ethylene Glycol-Capped Blue-Emitting Antimony Selenide Quantum Dots via Hydrothermal Approach. *Appl. Nanosci.* **2019**, *9* (4), 435−445.

https://doi.org/10.1021/acs.inorgchem.3c01799
Inorg. Chem. 2023, 62, 17102−17114

(49) Ou, X.; Yang, C.; Xiong, X.; Zheng, F.; Pan, Q.; Jin, C.; Liu, M.; Huang, K. A New RGO-Overcoated Sb2Se3 Nanorods Anode for Na + Battery: In Situ X-Ray Diffraction Study on a Live Sodiation/Desodiation Process. *Adv. Funct. Mater.* **2017**, *27* (13), No. 007.
(50) Černošková, E.; Todorov, R.; Černošek, Z.; Holubová, J.; Beneš, L. Thermal Properties and the Structure of Amorphous Sb 2 Se 3 Thin Film. *J. Therm. Anal. Calorim.* **2014**, *118* (1), 105−110.
(51) Doll, J. D.; Hu, B.; Papadimitrakopoulos, F. Precursor and Oxygen Dependence of the Unidirectional, Seeded Growth of CdSe Nanorods. *Chem. Mater.* **2012**, *24* (21), 4043−4050.
(52) Brown, H. C.; Mead, E. J.; Subba Rao, B. C. A Study of Solvents for Sodium Borohydride and the Effect of Solvent and the Metal Ion on Borohydride Reductions 1. *J. Am. Chem. Soc.* **1955**, *77* (23), 6209−6213.
(53) Ding, N.; Takabayashi, Y.; Solari, P. L.; Prassides, K.; Pcionek, R. J.; Kanatzidis, M. G. Cubic Gyroid Frameworks in Mesostructured Metal Selenides Created from Tetrahedral Zn2+, Cd2+, and in 3+ Ions and the [SbSe4]3- Precursor. *Chem. Mater.* **2006**, *18* (19), 4690−4699.
(54) Efthimiopoulos, I.; Zhang, J.; Kucway, M.; Park, C.; Ewing, R. C.; Wang, Y. Sb2Se3 under Pressure. *Sci. Rep.* **2013**, *3*, No. 02665.
(55) Nagata, K.; Ishibashi, K.; Miyamoto, Y. Raman and Infrared Spectra of Rhombohedral Selenium. *Jpn. J. Appl. Phys.* **1981**, *20* (3), 463−469.
(56) Kim, T. W.; Park, K. H.; Choi, Y. E.; Lee, J. Y.; Jung, Y. S. Aqueous-Solution Synthesis of Na3SbS4 Solid Electrolytes for All-Solid-State Na-Ion Batteries. *J. Mater. Chem. A* **2018**, *6* (3), 840−844.
(57) Eisenmann, B.; Zagler, R. Selenoantimonates(V): Preparation and Crystal Structure of Na3SbSe4, K3SbSe4 and [Ba(En)4] 2 [Ba(En)3](SbSe4) 2. *Z. Naturforsch. B* **1989**, *44* (3), 249−256.
(58) Smith, W. H.; Vaselabadi, S. A.; Wolden, C. A. Argyrodite Superionic Conductors Fabricated from Metathesis-Derived Li2S. *ACS Appl. Energy Mater.* **2022**, 14005. acsaem.2c00442
(59) Heo, S. H.; Jo, S.; Kim, H. S.; Choi, G.; Song, J. Y.; Kang, J. Y.; Park, N. J.; Ban, H. W.; Kim, F.; Jeong, H.; Jung, J.; Jang, J.; Lee, W. B.; Shin, H.; Son, J. S. Composition Change-Driven Texturing and Doping in Solution-Processed SnSe Thermoelectric Thin Films. *Nat. Commun.* **2019**, *10* (1), No. 187875.
(60) Li, D.; Li, R.; Qin, X.-Y.; Song, C.-J.; Xin, H.-X.; Wang, L.; Zhang, J.; Guo, G.; Zou, T.-H.; Liu, Y.-F.; Zhu, X.-G. Co-Precipitation Synthesis of Nanostructured Cu 3 SbSe 4 and Its Sn-Doped Sample with High Thermoelectric Performance. *Dalton Trans.* **2014**, *43* (4), 1888−1896.
(61) Kim, M.; Park, D.; Kim, J. Enhancement of the Thermoelectric Performance of Cu 3 SbSe 4 Particles by Controlling Morphology Using Exfoliated Selenium Nanosheets. *Dalton Trans.* **2022**, *51* (26), 10169−10178.
(62) Walker, B. C.; Agrawal, R. Contamination-Free Solutions of Selenium in Amines for Nanoparticle Synthesis. *Chem. Commun.* **2014**, *50* (61), 8331−8334.
(63) Wang, W.; Geng, Y.; Yan, P.; Liu, F.; Xie, Y.; Qian, Y. A Novel Mild Route to Nanocrystalline Selenides at Room Temperature. *J. Am. Chem. Soc.* **1999**, *121* (16), 4062−4063.
(64) Wei, Y.; Yang, J.; Lin, A. W. H.; Ying, J. Y. Highly Reactive Se Precursor for the Phosphine-Free Synthesis of Metal Selenide Nanocrystals. *Chem. Mater.* **2010**, *22* (20), 5672−5677.
(65) Webber, D. H.; Buckley, J. J.; Antunez, P. D.; Brutchey, R. L. Facile Dissolution of Selenium and Tellurium in a Thiol-Amine Solvent Mixture under Ambient Conditions. *Chem. Sci.* **2014**, *5* (6), 2498−2502.
(66) Deshmukh, S. D.; Easterling, L. F.; Manheim, J. M.; Libretto, N. J.; Weideman, K. G.; Miller, J. T.; Kenttämaa, H. I.; Agrawal, R. Analyzing and Tuning the Chalcogen-Amine-Thiol Complexes for Tailoring of Chalcogenide Syntheses. *Inorg. Chem.* **2020**, *59* (12), 8240−8250.
(67) Zhao, X.; Deshmukh, S. D.; Rokke, D. J.; Zhang, G.; Wu, Z.; Miller, J. T.; Agrawal, R. Investigating Chemistry of Metal Dissolution in Amine-Thiol Mixtures and Exploiting It toward Benign Ink Formulation for Metal Chalcogenide Thin Films. *Chem. Mater.* **2019**, *31* (15), 5674−5682.
(68) Antunez, P. D.; Torelli, D. A.; Yang, F.; Rabuffetti, F. A.; Lewis, N. S.; Brutchey, R. L. Low Temperature Solution-Phase Deposition of SnS Thin Films. *Chem. Mater.* **2014**, *26* (19), 5444−5446.
(69) Pavithraa, S.; Methikkalam, R. R. J.; Gorai, P.; Lo, J. I.; Das, A.; Raja Sekhar, B. N.; Pradeep, T.; Cheng, B. M.; Mason, N. J.; Sivaraman, B. Qualitative Observation of Reversible Phase Change in Astrochemical Ethanethiol Ices Using Infrared Spectroscopy. *Spectrochim. Acta, Part A* **2017**, *178*, 166−170.
(70) Tang, B.; Jaschin, P. W.; Li, X.; Bo, S. H.; Zhou, Z. Critical Interface between Inorganic Solid-State Electrolyte and Sodium Metal. *Mater. Today* **2020**, *41*, 200−218. December
(71) Deysher, G.; Chen, Y.; Sayahpour, B.; Lin, S. W.; Ham, S.; Ridley, P.; Cronk, A.; Wu, E. A.; Tan, D. H. S.; Doux, J.; Oh, J. A. S.; Jang, J.; Nguyen, L. H. B.; Meng, Y. S. Evaluating Electrolyte−Anode Interface Stability in Sodium All-Solid-State Batteries. *ACS Appl. Mater. Interfaces* **2022**, *14*, 47706.
(72) Tanibata, N.; Deguchi, M.; Hayashi, A.; Tatsumisago, M. All-Solid-State Na/S Batteries with a Na3PS4 Electrolyte Operating at Room Temperature. *Chem. Mater.* **2017**, *29* (12), 5232−5238.
(73) Wu, E. A.; Kompella, C. S.; Zhu, Z.; Lee, J. Z.; Lee, S. C.; Chu, I. H.; Nguyen, H.; Ong, S. P.; Banerjee, A.; Meng, Y. S. New Insights into the Interphase between the Na Metal Anode and Sulfide Solid-State Electrolytes: A Joint Experimental and Computational Study. *ACS Appl. Mater. Interfaces* **2018**, *10* (12), 10076−10086.
(74) Sahu, G.; Lin, Z.; Li, J.; Liu, Z.; Dudney, N.; Liang, C. Air-Stable, High-Conduction Solid Electrolytes of Arsenic-Substituted Li4SnS4. *Energy Environ. Sci.* **2014**, *7* (3), 1053−1058.

https://doi.org/10.1021/acs.inorgchem.3c01799
Inorg. Chem. 2023, 62, 17102−17114